Self- and Solute Diffusion, Interdiffusion and Thermal Vacancies in the System Iron-Aluminium

Helmut Mehrer[1,a], Martin Luckabauer[2], and Wolfgang Sprengel[2]

[1]Institute of Materials Physics, University of Münster, D-48419 Münster
Wilhelm-Klemm Str. 10, Germany

Private address: D-73635 Obersteinenberg, Berghof 3, Germany

[2]Institute of Materials Physics, Graz University of Technology, A-8010 Graz
Petersgasse 16, Austria

[a]mehrer@uni-muenster.de

Keywords: Iron, aluminium, iron-aluminium alloys, self-diffusion, solute diffusion, interdiffusion, defects, thermal vacancies, vacancy migration, differential dilatometry, positron annihilation

Abstract. Starting from fundamental aspects of thermal vacancies and solid-state self- and solute diffusion, this paper reviews procedures for tracer- and interdiffusion studies and of the major techniques for vacancy studies by dilatometry and positron annihilation in metals. Equilibrium vacancy and diffusion studies performed on pure iron and aluminium are mentioned at first. We also comment some peculiarities of solute diffusion in aluminium. Positron annihilation and differential dilatometry studies for Fe-Al alloys with various compositions are summarized and new experimental studies by the authors are reported for vacancy migration in $Fe_{61}Al_{39}$. All these studies indicate a relatively high fraction of thermal vacancies with relatively low mobility in this type of iron-aluminides as compared to pure metals. Tracer diffusion of iron and of several substitutional solutes such as Co, Ni, Cr, Mn, Zn, and In in Fe-Al from the Münster laboratory are summarized. The diffusion studies of Fe-Al cover various alloy composition between Fe_3Al and FeAl and several structures such as A2, B2 and $D0_3$. Interdiffusion coefficients obtained from diffusion couples between Fe-Al alloys are discussed together with Fe tracer diffusion data. The Darken-Manning equation is used to deduce Al diffusivities therefrom. The latter are hardly accessible to radiotracer experiments due to a lack of a suitable Al tracer. Diffusion of Al is slightly faster than diffusion of Fe indicating diffusion mechanisms with coupled jumps of Fe and Al atoms.

Introduction

Iron and aluminium as well as iron-aluminium alloys are very important metallic materials because of their outstanding physical, chemical and mechanical properties and their relatively low costs. Iron is the second-most abundant element on our planet. It is, with about 95 %, by far the most frequently used metallic element in technology either in the form of steels or as cast iron. Aluminium is after silicon and oxygen the third-frequent element in the earth crust. It is used in the form of cans and foils in packing technology, as an excellent electric conductor, in aluminium-alloys as light-weight construction materials of aeroplanes and cars and in many other fields.

Alloys on the basis of iron and aluminium are of high technological interest as high-temperature structural materials due to their excellent corrosion and oxidation resistance. In

comparison with conventional steels they also have a higher specific strength combined with an up to 20 % lower density [1].

Diffusion in solids is fundamental in the art and science of materials and an important topic of solid-state physics, physical metallurgy and materials science. A deeper knowledge about diffusion requires information on the positions of atoms and how they move in solids. In crystalline solids the atomistic mechanisms of diffusion are closely connected with point defects in equilibrium, such as vacant lattice sites, which mediate self-diffusion and diffusion of many substitutional solutes in metals. Dislocations and grain boundaries are other types of defects and can act as high-diffusivity paths /also called diffusion short-circuits), because the mobility of atoms along such defects is usually much higher than in the lattice. The influence of diffusion short-circuits must be carefully considered to obtain reliable bulk diffusion data. Self-diffusion is the most basic diffusion process in any solid. Diffusion of solutes is relevant for the behaviour of alloying elements. For comprehensive insights into the field of diffusion we refer the reader to the textbooks of Philibert [2] and one of the authors [3].

We remind the reader in section 2 of some basic facts about thermal vacancies, self- and solute diffusion. Section 3 is devoted to the major techniques for studies of thermal vacancies, tracer diffusion and interdiffusion. We then summarize in sections 4 and 5 facts available in the literature about self-diffusion and thermal defects for both elements iron and aluminium and we comment on the peculiarities of solute diffusion in aluminium. Then we proceed in sections 6 and 7 to a discussion of formation and migration of vacancy-type defects, self-diffusion, interdiffusion, and solute diffusion in iron-rich Fe-Al alloys.

Some remarks about thermal vacancies, self- and solute diffusion

Usually, in metals the dominating point defects in thermal equilibrium are vacant lattice sites. Since their site fraction in equilibrium increases with temperature, at temperatures above about 2/3 of the melting temperature agglomerates of single vacancies, such as divacancies, may come into play as well. The fraction of vacant sites, C_V, and the tracer self-diffusivity, D^T, are given by:

$$C_V = C_{1V} + 2C_{2V} + ... \Leftrightarrow D^T = D_{1V}^T + D_{2V}^T + ... \quad . \tag{1}$$

Here C_{1V} and C_{2V} denote the site fractions of mono- and divacancies and ${D_{1V}}^T$ and ${D_{2V}}^T$ their contributions to the tracer self-diffusivity. In the following we refrain from discussing complications due to divacancies and higher agglomerates and explain the basic facts by referring to monovacancies. In a careful analysis of data of pure metals divacancies must sometimes be taken into account. For details, we refer the reader to a paper by Seeger and Mehrer [4]. As we shall see below thermal vacancy site fractions in Fe-Al alloys can be fairly high. Therefore agglomerates of vacant sites such as vacancy pairs and triple defects (two vacancies in one sublattice and an antisite atom in the other sublattice) may be more important than in pure metals.

If monovacancies are the dominant species of vacant sites, which is always the case at lower temperatures, their site fraction is given by:

$$C_{1V} = \exp(S_{1V}^F / k_B) \exp(-H_{1V}^F / k_B T), \tag{2}$$

where S_{1V}^F and H_{1V}^F denote the entropy and enthalpy of vacancy formation, k_B the Boltzmann constant, and T the absolute temperature. Self-diffusion (measured by tracers, i.e. by isotopes of the same element) occurs by exchange jumps of tracer atoms with neighbouring vacant sites. The self-diffusion coefficient mediated by monovacancies in a cubic crystal is given by

$$D_{1V}^{T} = f_{1V} a^2 C_{1V} \nu_{1V} = f_{1V} a^2 \nu_{1V}^{0} \exp[(S_{1V}^{F} + S_{1V}^{M})/k_B] \exp[-(H_{1V}^{F} + H_{1V}^{M})/k_B T]. \quad (3)$$

Here f_{1V} denotes the correlation factor, which in simple cases is just a number, e.g. 0.781 for a monovacancy mechanism in an fcc lattice and 0.727 in a bcc lattice. ν_{1V} denotes the jump rate of the vacancy and ν_{1V}^{0} the pertaining attempt frequency (of the order of the Debye frequency) S_{1V}^{M} and H_{1V}^{M} denote the entropy and enthalpy of vacancy migration. The activation enthalpy of self-diffusion for a monovacancy mechanism is:

$$Q_{1V} = H_{1V}^{F} + H_{1V}^{M} \approx Q, \quad (4)$$

i.e. the sum of formation and migration enthalpies of the vacancy. As long as agglomerates can be neglected, Eq.(4) represents the total activation enthalpy Q of self-diffusion.

Self-diffusivities in fcc metals near the melting temperature lie between 10^{-12} m^2s^{-1} and 10^{-13} m^2s^{-1}. If the self-diffusivities of fcc metals are plotted in an Arrhenius diagram with a temperature scale normalized to the respective melting temperature, the self-diffusivities of all fcc metals lie in a relatively narrow band. This implies that the ratio between the activation enthalpies Q and the melting temperatures T_m of all fcc metals is similar:

$$Q_{1V} \approx Q = (15 \text{ to } 19)\, k_B T_m, \quad (5)$$

In the spectrum of self-diffusivities of fcc metals aluminium is on the top [3]. For bcc metals the self-diffusivities near the melting temperature are typically one order of magnitude higher than in fcc metals and the spectrum of self-diffusivities in the normalized Arrhenius plot is wider [3].

Substitutional solutes in a metal diffuse via a vacancy-type mechanism as well. Solute diffusion in a very diluted alloy is called *impurity diffusion*. In this case, it is justified to assume that impurity atoms are isolated, i.e. formation of solute pairs, triplets, etc. is negligible. The theory of vacancy-mediated impurity diffusion was developed by Lidiard [5] and LeClaire [6] half a century ago. It takes into account the interaction between impurity and vacancy and the influence of the impurity on the neighbouring solvent atoms. The probability for a vacancy to occupy a nearest-neighbour site of a solute is given by:

$$p = C_{1V} \exp(G_B/k_B T) = \exp[(S_{1V}^{F} - S^{B})/k_B] \exp[-(H_{1V}^{F} - H_B)/k_B T], \quad (6)$$

where $G^B = H^B - TS^B$ is the Gibbs free energy of solute-vacancy interaction. For $G^B > 0$ the interaction is attractive, for $G^B < 0$ it is repulsive. The impurity diffusion coefficient D_2 of vacancy-mediated diffusion in an fcc lattice can be written as

$$D_2 = f_2 a^2 \omega_2 p = f_2\, a^2 \omega_2 C_{1V} \exp[G^B/k_B T]. \quad (7)$$

Here f_2 is the impurity correlation factor and ω_2 the vacancy-impurity exchange rate. In contrast to self-diffusion, it is necessary to consider for impurity diffusion several atom-vacancy exchange rates with atoms in the vicinity of the impurity atom. Five types of exchanges, between vacancy, impurity, and host atoms are introduced in the 'five-frequency model'. The impurity correlation factor is no longer a constant as in the case of self-diffusion. It depends on the various jump rates of the vacancy. The impurity correlation factor can be written as (see, e.g. [3])

$$f_2 = \frac{\omega_1 + 7F_3\omega_3/2}{\omega_2 + \omega_1 + 7F_3\omega_3/2}. \quad (8)$$

ω_1 is the rotation rate of the solute-vacancy complex, ω_3 and ω_4 denote rates of dissociation and association of this complex. The escape probability F_3 is a function of the ratio ω / ω_4, where ω denotes the vacancy jump rate in the pure solvent. The detailed balance condition demands that $\omega_3 / \omega_4 = exp\ (G^B/k_BT)$. Hence the impurity diffusion coefficient can be written as:

$$D_2 = f_2 a^2 \nu^0 \exp[(S_{1V}^F - S^B + S_2^M)/k_B] \exp[-(H_{1V}^F - H^B + H_2^M)/(k_B T)], \quad (9)$$

where H^B and S^B denote the binding enthalpy and entropy of the vacancy-impurity complex and H_2^M and S_2^M enthalpy and entropy of the vacancy-impurity exchange jump ω_2. The ratio of the diffusion coefficients of impurity and self-diffusion can be written as:

$$\frac{D_2}{D^T} = \frac{f_2}{f_{1V}} \frac{\omega_2}{\omega} \frac{\omega_4}{\omega_3}. \quad (10)$$

This equation shows that the diffusion coefficient of a substitutional impurity differs from the self-diffusion coefficient of the pure solvent for three reasons: (i) correlation effects, (ii) differences in the vacancy exchange rates between impurity and solvent atoms, and (iii) interaction between impurity and vacancy.

Since solute and solvent atoms are located on the same lattice and since the diffusion of both is mediated by vacancies, often a relatively small diffusivity dispersion between solvent and solute diffusion – often less than two order of magnitude -- is observed for many fcc metals. It reflects the high efficiency of screening of point charges in the solvent metal, which normally limits the vacancy-impurity interaction enthalpy H^B to fairly small values between 0.1 and 0.3 eV. Such values are small relative to typical vacancy formation enthalpies. However, we shall see below that the dispersion in impurity diffusion in the tri-valent aluminium provides an exception from this rule. This is mainly due to the fairly strong interaction between transition-metal solutes and the aluminium vacancy.

Procedure for studies of thermal vacancy properties, tracer diffusion and interdiffusion – a reminder

The basic point defects in solids are vacancies and self-interstitials. For high-temperature and diffusion properties in metals and intermetallics the formation of vacant lattice sites in thermal equilibrium are of particular importance, because the formation enthalpy of self-interstitials is significantly higher than that of vacancies. Hence, the concentration of vacant sites, C_V, is much higher than the thermal concentration of self-interstitials, which usually can be neglected under equilibrium conditions.

The only direct experimental procedure for the measurement of the site fraction of vacant lattice sites is *differential dilatometry*. Differential dilatometry requires the simultaneous measurement of the relative change of the macroscopic volume, $\Delta V/V$, and of the relative change of the microscopic volume, $\Delta\Omega/\Omega$. For crystals without any or with negligible concentrations of self-interstitials the basic equation can be written as:

$$\Delta V/V - \Delta\Omega/\Omega = 3(\Delta l/l - \Delta a/a) = C_V. \quad (11)$$

For cubic crystals, the volume changes can be obtained from measurements of the changes of the lattice parameter, $\Delta a/a$, and changes of the specimen length, $\Delta l/l$. Successful differential dilatometry studies require high precision for both quantities, because the fractions of vacant lattice sites are often very small numbers. However, this technique has the great advantage that it neither introduces an unknown constant of proportionality nor requires empirical elimination of background effects. Differential dilatometry has been successfully applied to study several pure metals, including aluminium and to a few binary alloys including Fe-Al alloys (see Sect. 6.2).

We note, however, that differential dilatometry registers nothing but the total vacancy content of a solid. Whether vacancies are present as isolated vacancies or as agglomerates cannot be deduced from such measurements. Differential dilatometry also cannot distinguish on which sublattice of an intermetallic compound vacant sites are located.

Equilibrium defects in metals can also be studied by positron annihilation techniques (see, e.g., [7]. For the investigation of thermal vacancies the annihilation of positrons with electrons of the solid and the detection of the annihilation radiation is a sensitive technique. In *positron lifetime experiments*, the time between the injection of a positron into a solid and the detection of the positron-electron annihilation γ-quantum is used to deduce the positron lifetime. In such studies often proton-rich, radioactive isotopes are used as positron sources where the emission of the positron is accompanied, quasi simultaneously, by the emission of a gamma quantum. This prompt gamma quantum is then used to mark the time of the positron injection. In the case of the application of a positron beam, pulsed positron beams have to be used for positron lifetime measurements.

In metals, vacancies act as traps for positrons. If a positron gets trapped and localized in a vacancy it encounters an electron density different from the delocalized state of the defect-free lattice. Usually the lifetime of a positron increases if it is trapped in a vacancy because the electron density in a vacancy is lower due to the missing core electrons compared to the interstitial sites of the perfect lattice. Therefore, the mean positron lifetime increases when thermal vacancies are formed in a metal giving an S-shaped (or sigmoidal) curve with increasing temperature. From an analysis of such data the formation enthalpy of vacancies can be deduced.

In the framework of the simplest model, the two-state trapping model, the mean positron life-time $\bar{\tau}$ is given by:

$$\bar{\tau}(T) = \tau_f \frac{1 + \sigma C_V \tau_t}{1 + \sigma C_V \tau_f}, \tag{12}$$

where τ_f and τ_τ denote the lifetimes of positrons annihilating in the undisturbed lattice (‘free’ positrons, index *f*) or in the traps (index *t*), respectively and σ denotes the specific trapping rate for positrons and C_V denotes the site fraction of traps, i.e., the fraction of vacant sites.

In a careful analysis of positron data, small intrinsic temperature dependencies of the lifetimes and of the trapping rate must also be taken into account, see, e.g., straight line in Fig. 6. Furthermore, in some metals, but not for iron and aluminium, the possibility of de-trapping of positrons from vacancies must be considered as well. We refrain from a detailed discussion of these effects and refer to the positron annihilation literature instead. However, it is obvious from above, that only the product σC_V and not the thermal vacancy fraction itself can be determined in positron experiments.

Analysis of the *Doppler broadening of the 2γ positron-annihilation line* gives access to the electron momentum distribution around the positron annihilation site and can be applied for the study of vacancies as well. The low electron momentum region results from annihilation events with valence electrons whereas annihilation events with core electrons

will contribute to the high electron momentum range. Often so-called S- and W-parameters are determined, which are deduced as fraction of annihilation events with valence electrons in specific low-electron momentum range and with core electrons in a specific high-electron momentum range, respectively. In the presence of thermal vacancies all quantities, mean positron life-time and S-parameter as well as W-parameter reveal characteristic shapes as a function of temperature.

For binary ordered compounds one additional aspect of positron annihilation with core electrons is of importance. From positron lifetime studies alone it is nearly impossible to elucidate the sublattice on which vacancies predominantly form. Fortunately, here the Doppler broadening of the annihilation line measured for both annihilation quanta in coincidence can be used to determine the electron momentum distribution up to the relatively high momenta of the core electrons. In this way, the atoms surrounding a vacancy can be analysed specifically giving access to the local chemical environment of a vacancy. Thereby the sublattice on which a vacancy is formed in an ordered intermetallic compound may be identified see, e.g. [29].

Many of the reliable diffusion studies on solids are performed by *radiotracer techniques*. For self-diffusion studies radioisotopes of the same element are used, for solute diffusion studies radioisotopes of the solute element are employed. The tracer is deposited as a thin layer onto a carefully polished flat surface of the sample. After the tracer deposition an isothermal diffusion anneal is performed at temperature T for some diffusion time t either under protective atmosphere or in vacuum. Then the concentration distribution as function of the penetration depth x, $C(x,t)$, is usually described by the thin-film solution of Fick's second law:

$$C(x,t) = \frac{M}{\sqrt{\pi D^T t}} \exp(-x^2 / 4D^T t) \,. \tag{13}$$

The quantity $\sqrt{D^T t}$ is a typical diffusion length. In a tracer diffusion experiment the depth distribution of the in-diffused tracer is usually measured by taking a series of thin sections and measuring the radioactivity of each section by a suitable nuclear counting technique. The latter is proportional to the tracer concentration. Mechanical sectioning methods are in use for large enough diffusion lengths. For small diffusion lengths, which usually occur in studies at lower diffusion temperatures, sputter sectioning has often been applied successfully. Details about the radiotracer method can be found, e.g. in the textbook of Mehrer [3].

As examples, we show in Fig.1 penetration profiles of ^{59}Fe into iron single crystals obtained by sputter sectioning. In the left part of Fig.1 the thin-film solution is observed over several orders of magnitude in concentration. This permits a determination of the diffusivities by fits of Eq. (13) with good precision. Deviations from the thin-film behaviour can be seen in the right part of Fig. 1, which was also measured on an iron single crystal. The part near the surface is due to bulk diffusion whereas the deeper penetrating tail is caused by dislocation pipe diffusion. Fig. 1 illustrates an additional great virtue of the radiotracer method, in addition to its high sensitivity: it is capable of distinguishing between bulk and short-circuit diffusion processes.

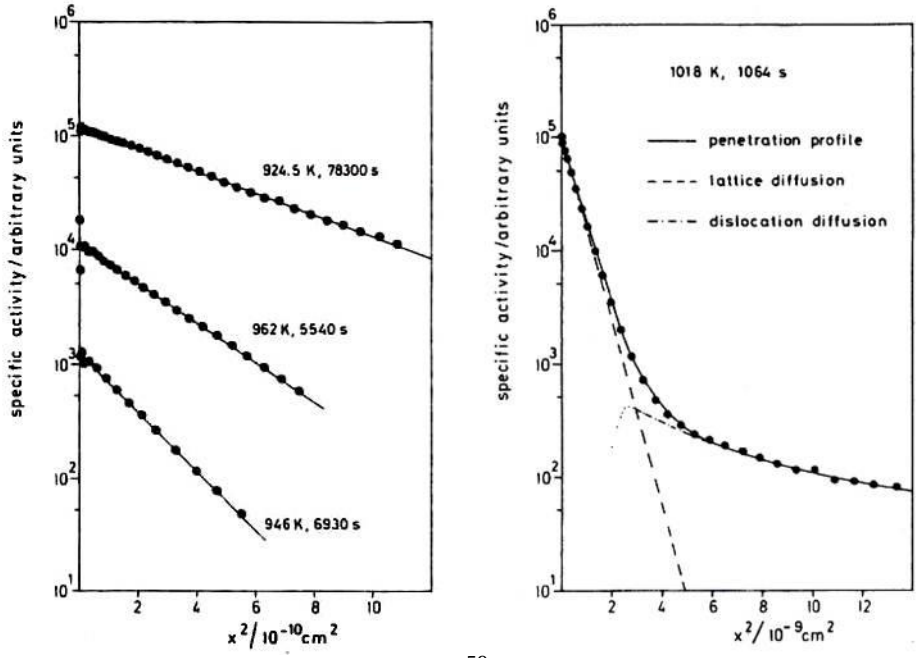

Fig. 1: Penetration profiles of the radioisotope ^{59}Fe in iron single crystals obtained by sputter sectioning according to Lübbehusen and Mehrer [8]. Left panel: The profiles are caused by bulk self-diffusion and the solid lines represent thin-film solutions. Right panel: The profile is caused by bulk self-diffusion in the near-surface region. The deeper penetrating tail represents dislocation- pipe diffusion.

A different type of diffusion experiment is an *interdiffusion study*. In an interdiffusion study one considers a binary diffusion couple of two elements or two alloys with different compositions. In a diffusion anneal the chemical composition varies due to diffusional intermixing in the diffusion zone. Diffusing atoms experience different chemical environments and hence their diffusion coefficients vary with composition and distance *x*. The composition profile can be measured, e.g., by electron microprobe analysis. The Boltzmann-Matano method permits to determine a composition-dependent interdiffusion coefficient, D_{int},, from the composition-distance profile, $C(x)$, via

$$D_{\mathrm{int}}(C^*) = -\frac{1}{2t}\frac{\int_{C_0}^{C^*}(x - x_M)dC}{(dC/dx)_{C^*}}. \qquad (14)$$

Here C^* is the concentration at the chosen composition, C_0 the initial composition, say at the left-hand side of the diffusion couple, and x_M the position of the so-called Matano plane. The position of the Matano plane is not known a priori but can be found from the experimental composition distance profile. For details see textbooks on diffusion [2, 3]. The interdiffusion coefficient is related – for a random alloy -- via the Darken-Manning equation to the tracer diffusion coefficients, D_A^T and D_B^T, of the components A and B via

$$D_{\mathrm{int}} = (N_A D_B^* + N_B D_A^*)\Phi S\,. \qquad (15)$$

Here N_A and N_B denote the atomic fractions of the components and Φ the thermodynamic factor. The vacancy-wind factor S is of the order of unity and thus often a small correction. Equation (15) can be used to determine the tracer diffusion coefficient of one of the components if the other tracer diffusivity has been measured. In particular, one can take

advantage of this idea in the case of aluminium alloys such as Fe-Al as discussed below. The tracer diffusivity of iron can be determined in tracer experiments, whereas the tracer diffusivity of aluminium is very hard to obtain because no suitable tracer for Al is accessible nowadays. To this end the thermodynamic factor must be either measured or obtained from theoretical calculations.

Self-diffusion and thermal vacancies in iron

Pure iron undergoes several phase transitions with varying temperature. Bcc α-Fe exists below 1183 K, γ-Fe is fcc and exists between 1183 and 1653 K. Above 1653 K up to the melting temperature of 1809 K δ-Fe is bcc. The two bcc-fcc structural transitions are first order phase transitions. Below the Curie temperature of 1043 K α-Fe becomes ferromagnetic, above it is paramagnetic. The magnetic transition is a typical second-order phase transition.

Self-diffusion: Self-diffusion in pure iron has been studied using radiotracer techniques by several groups. All phase transitions mentioned above are reflected in the temperature dependence of self-diffusion shown in Fig. 2. The figure shows that the two first order transitions from the close-packed structure of γ-Fe to the less densely packed bcc structures of the α-Fe and δ-Fe phases are accompanied by abrupt increases in self-diffusivity. In the close-packed fcc structure diffusion is slower at similar temperatures than in the more open bcc structure. A second-order transition (here: from paramagnetic to ferromagnetic order) is characterized by an order parameter (here: the spontaneous magnetization), which varies in a continuous manner with temperature. Self-diffusion varies continuously with temperature from the paramagnetic to the ferromagnetic state as well. Below the Curie temperature, the activation enthalpy increases and self-diffusion is slower than an extrapolation from the paramagnetic state would suggest.

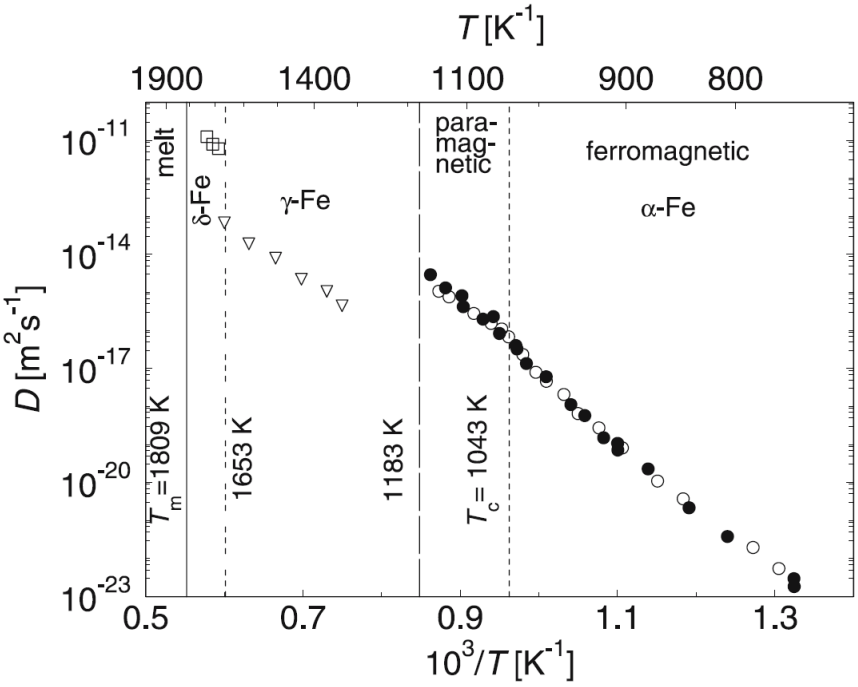

Fig. 2: Arrhenius diagram of self-diffusion in the various phases of iron according to Mehrer [3]. Full circles [8], open circles [9], triangles [10], squares [11].

Thermal vacancies. Differential dilatometry studies for iron are not available to the authors' knowledge. However, equilibrium vacant sites in iron have been studied by Doppler broadening positron annihilation techniques by Schaefer and co-workers [12, 13]. The W-parameter of the annihilation line is displayed in Fig.3 as a function of temperature. It is

discontinuous at the structural phase transitions and larger in the fcc phase. This indicates that vacancy trapping is more pronounced in the bcc phase than in the fcc phase. Trapping of positrons starts at about 1050 K, slightly above the Curie temperature. Below 1050 K the concentration of vacancies is too low and positrons do not find a vacant site during their short life (about 100 ns) and annihilate from defect-free sites in iron. The W-parameter saturates near the melting temperature, where the vacancy concentration is high enough to provide a trap for each positrons. Formation enthalpies of vacancies around 1.5 eV have been deduced. For a detailed discussion we refer to the papers of Schaefer et al. [12] and Maier et al. [13].

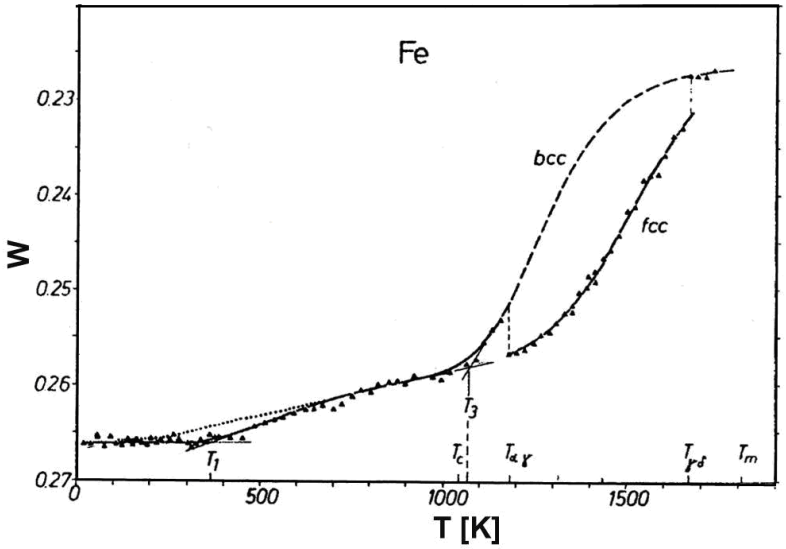

Fig. 3: Positron annihilation line-shape parameter W of iron as a function of temperature according to Schaefer et al. [12].

Diffusion and thermal vacancies in aluminium

Self-diffusion in aluminium. Aluminium crystallises in the fcc structure up to its melting temperature. Self-diffusion in aluminium has been studied over a wide temperature range by combining various experimental techniques (Fig. 4). At high temperatures radiotracer experiments have been performed employing the then still available very long-lived tracer ^{26}Al [15]. Unfortunately, ^{26}Al is the only radiotracer of aluminium with an extremely long half-life and hence a very bad specific activity, which seriously limits diffusion experiments. In a middle temperature range spin-lattice relaxation NMR techniques have been successfully used to deduce self-diffusivities of Al [16]. At low temperatures the shrinkage of voids was observed in a transmission electron microscope. From the shrinking kinetics self-diffusivities were deduced [17]. Both techniques, NMR and void shrinkage, are less direct than tracer studies. Both require theoretical models.

Thermal vacancies in aluminium. Aluminium has been studied by two groups by means of differential dilatometry. The results have been collected by Seeger and Mehrer [4] and are shown in Fig.5. Figure 5 also includes calorimetric measurements, in which the specific heat is determined as a function of temperature. In such experiments the 'constant of proportionality' is the formation enthalpy of a vacant site. However, the background problem remains, which makes this method less direct than differential dilatometry. The data in Fig.5 from the various groups are in good agreement and reveal fractions of vacant sites around 9×10^{-4} near the melting temperature. This value which is the highest number observed for an fcc metals [4]. This high value has suggested that vacancy clusters such as divacancies contribute to the total vacant lattice site fractions and also to self-diffusion in aluminium as discussed in detail in [4].

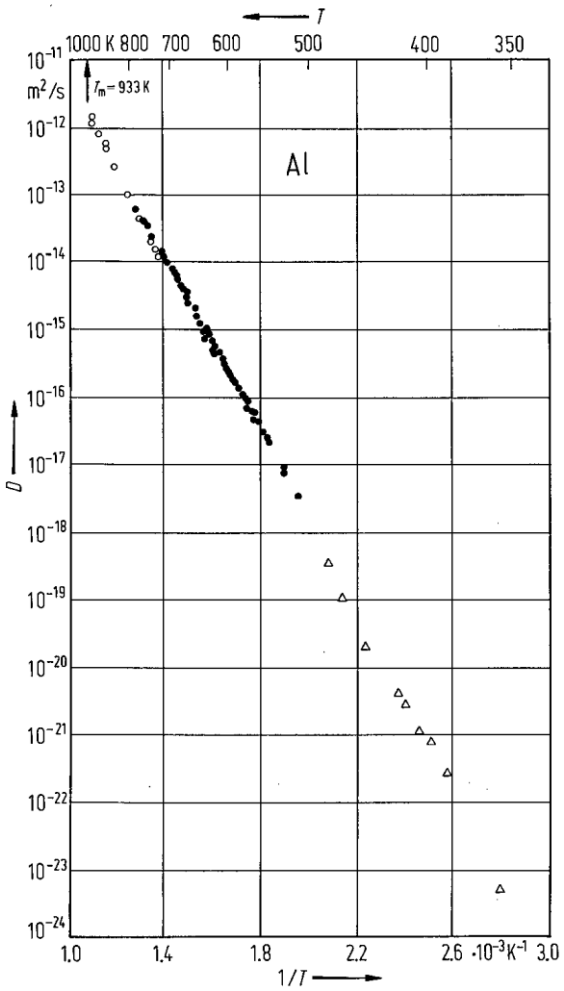

Fig. 4: Self-diffusion data for aluminium taken from the collection of diffusion data edited by Mehrer [14]. Open circles: radiotracer experiments with ^{26}Al [15], full circles: NMR studies [16], triangles: TEM observation of shrinkage of voids [17].

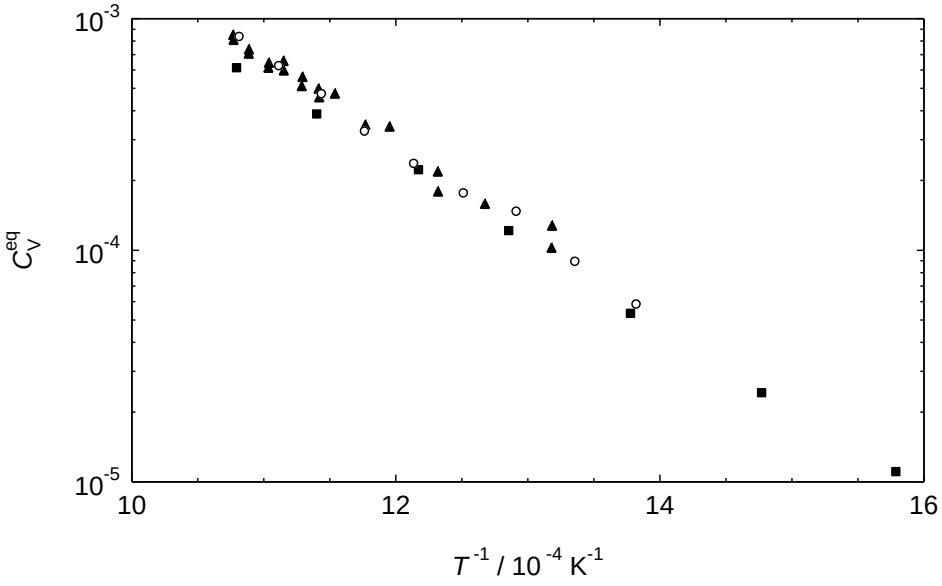

Fig. 5: Equilibrium fractions of vacant lattice sites for pure aluminium (redrawn from Seeger and Mehrer [4]). Data are from: differential dilatometry [18] (open circles), differential dilatometry [19] (triangles), and calorimetric measurements assuming a value of 0.65 eV for the formation enthalpy of a vacancy [20] (full circles).

Positron lifetime measurements have been used as well to study thermal vacancies in high-purity aluminium [21]. The mean lifetime of positrons is shown in the left part of Fig. 6 as a function of temperature. The data reveal the sigmoidal temperature dependence predicted by the two-state trapping model.

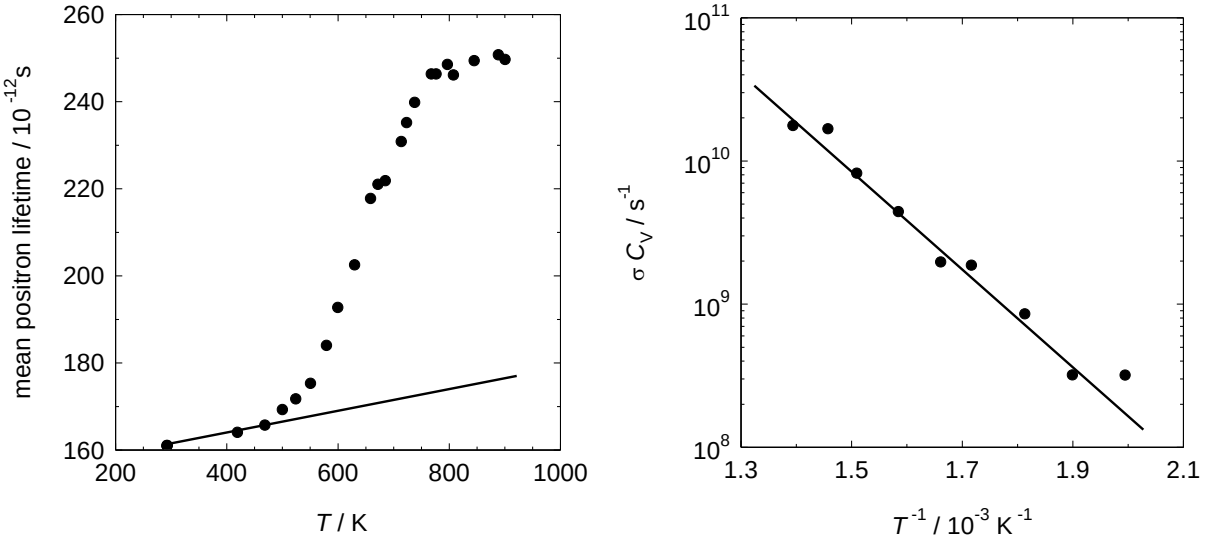

Fig. 6: Left panel: Mean positron lifetime in aluminium as function of temperature according to Schaefer et al. [21]. The solid line indicates the temperature dependence of the positron lifetime in the delocalized, defect-free state. Right panel: Arrhenius diagram of the product $\sigma\, C_V$ in aluminium according to [21] where σ denotes the specific vacancy trapping rate of a positron and C_V the concentration of thermal vacancies. An activation enthalpy H_V^F of 0.68 eV for thermal vacancy formation is deduced from the data.

From a fit of Eq. (12) to the lifetime data the product σC_V has been deduced in Ref. [21]. It is shown in the Arrhenius diagram on the right panel of Fig. 6. The slope of the line represents an activation enthalpy of 0.68 eV, a value which is mainly attributed to the formation of vacant lattice sites. However, this value may require a small correction arising from a small temperature dependence of the positron trapping rate σ.

Solute diffusion in aluminium. In contrast to the monovalent and fcc noble metals Al is trivalent and the diffusion of impurities in Al is remarkably different from that of impurities in noble metals mentioned in Section 2. Figure 7 shows on the left side an Arrhenius diagram for impurity diffusion data in Al together with Al self-diffusion data. A striking feature of this figure is that most transition metals (V, Ti, Cr, Mn, Fe) exhibit extremely low diffusivities with respect to Al self-diffusion. In addition, they have high activation enthalpies and they also have high pre-exponential factors. Non-transition elements (Ge, Ga, Zn) have diffusivities similar or slightly higher than self-diffusion and the data show only small variations for the different elements. Their activation enthalpies are similar to those of Al self-diffusion and almost independent of their valence.

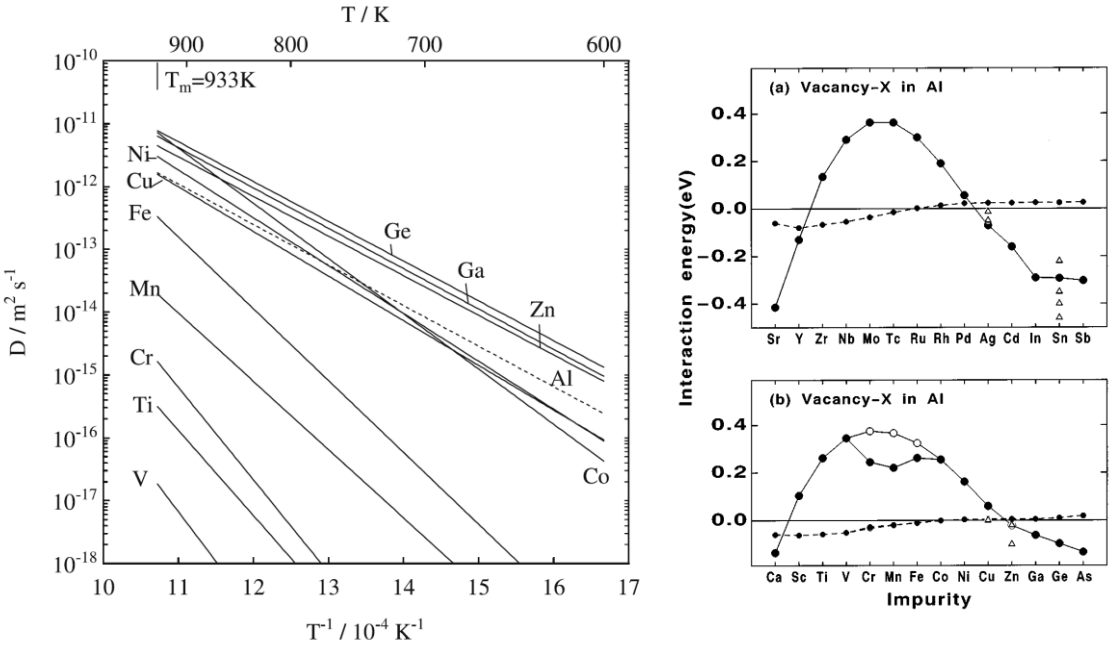

Fig. 7: Left panel: Arrhenius diagram for diffusion of various solutes in aluminium according to Mehrer [3]. The dashed line represents self-diffusion in aluminium. Right panel: Vacancy-solute interaction in aluminium from local-density calculations of Hoshino et al. [22]. Full lines: 3d and 4d solutes; dashed lines: 4sp and 5sp solutes.

The reason for the deviation of diffusivities of transition metals from 'normal' impurity diffusion behaviour of other fcc metals very likely lies in the fairly strong interaction between vacancy and solute atoms. This can be seen from the calculations of vacancy-solute interaction energies for 3d and 4sp as well as 4d and 5sp element solutes performed by Hoshino et al. [22]. The results are displayed in the right part of Fig.7. The interaction is repulsive for most transition element solutes and attractive for non-transition element solutes. Unfortunately, according to the authors' knowledge there are no calculations of the activation enthalpy of the vacancy-solute exchange H_2^M, which according to Eq. (9) contributes to the activation enthalpy of impurity diffusion. H_2^M could be fairly high for transition metals as well.

Thermal vacancies and diffusion in Fe-rich Fe-Al alloys

Some Fe-Al phases and their structures. An overview of the iron-aluminium phases is given by the binary Fe-Al phase diagram shown in Fig.8. There are two slightly different versions of the Fe-Al diagram, one summarized by Kubaschewski [23] and a slightly different one by Massalski [24]. In the Kubaschewski version of the diagram a subdivision of the B2-phase region, indicated by the dashed lines in Fig.8, was proposed according to observed changes in some physical properties such as thermal expansion, specific heat and elastic moduli reported by Köster and Gödecke [25]. These changes are not accompanied by changes in crystal symmetry or atomic order. However, they have influences on the defect population as we shall see below. In the Massalski version of the phase diagram this subdivision is omitted.

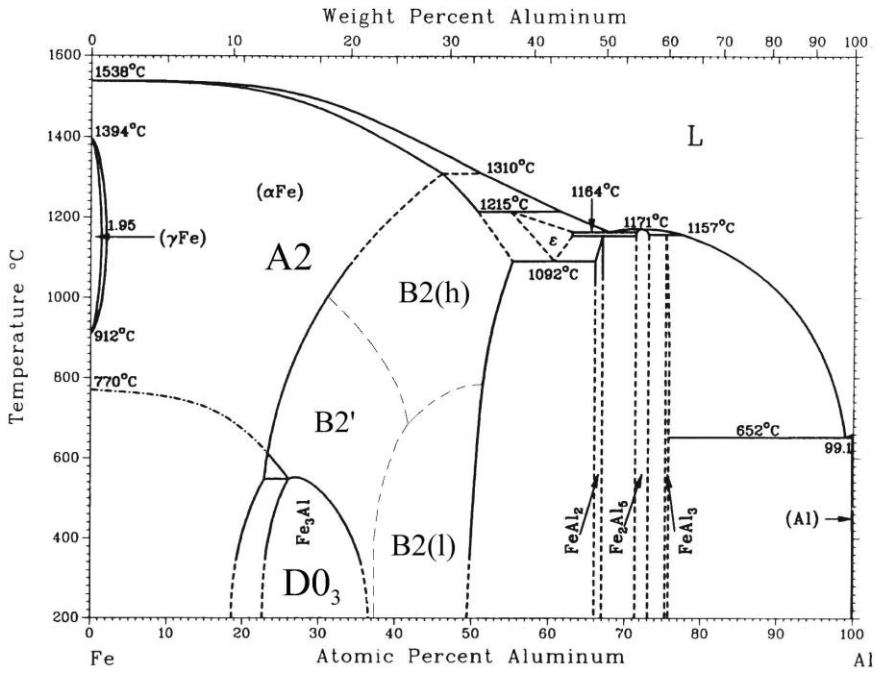

Fig. 8: Phase diagram of the binary iron-aluminium system according to Kubaschewski [23]. The B2-ordered phase field is subdivided by dashed lines.

The phase diagram shows several intermetallic phases of Fe and Al: a disordered bcc phase A2, an ordered B2-phase (subdivided in the Kubaschewski diagram into B2(h), B2(l) and B2' by dashed lines), and a $D0_3$ ordered phase around the composition Fe_3Al Three Al rich phases $FeAl_2$, Fe_2Al_5, and $FeAl_3$ are of interest for Al-base alloys. They are not addressed in this paper. Only diffusion and vacancies in the Fe-rich iron-aluminides A2-FeAl, B2-FeAl and Fe_3Al will be considered

The A2-structure is a more or less random distribution of Fe and Al atoms on a bcc lattice. The B2-structure is cubic as well and can be derived from the bcc lattice, if the two primitive cubic sublattices are occupied mainly by different kinds of atoms like in the CsCl-type structure. The $D0_3$ structure is also cubic with the approximate composition Fe_3Al. It can be viewed as an ordered structure derived from the bcc lattice as well. B2-FeAl, like B2-NiAl is formed by an ordering process from the disordered A2 structure. The order-disorder transition temperature increases with Al-content. B2-ordered FeAl, in contrast to B2-NiAl, melts incongruently. Both alloys, B2-FeAl like B2-NiAl, are considered to have high potential as high-temperature structural material. Both B2-phases also form a continuous ternary solid solution. Fe_3Al is formed on cooling by ordering reactions that transform disordered A2-FeAl, which is stable above 800°C, first into a B2-FeAl phase and then into Fe_3Al with the $D0_3$ structure. Fe_3Al exhibits a high magnetic permeability, which makes it useful as a magnetic material.

Thermal vacancies in Fe-rich iron-aluminides. In principle, point defects in ordered intermetallics comprise a variety of constitutional defects, such as vacancies in each sublattice, as well as antisite defects in each sublattice. Also agglomerates of these basic defects such as vacancy pairs and triple defects may occur. A triple defect consists of two vacancies on one sublattice and an antisite atom on the other sublattice. With respect to vacancies two different types may be distinguished as well: constitutional and thermal vacancies. In some intermetallics constitutional vacancies are necessary to compensate for off-stoichiometry. In other intermetallics antisite defects compensate off-stoichiometry

In the case of B2 intermetallics such as NiAl and FeAl embedded atom calculations by Fu et al. [26] and ab-initio calculations by Fähnle et al. [27] provided insights into the defect structure: Antisite atoms are the structural defects on the Fe-rich and the Al-rich side of FeAl. In iron-rich aluminides the compensation of off-stoichiometry is mainly due to Fe antisite defects. The site fraction of thermal vacancies on the transition-metal sublattice of B2 FeAl has been predicted to exceed that on the Al sublattice considerably, because the Al vacancy has a large formation enthalpy.

Fortunately, the question on which sublattice of B2-FeAl thermal vacancies are formed has received an experimental answer as well. Müller et al. [28] studied vacancies by coincident measurements of the 511 keV positron-electron photon annihilation line. This technique permits to detect electron momenta up to the high values characteristic for core electrons. Such measurements allow for a chemical discrimination of the atoms located in the vicinity of the positron annihilation site. For a positron trapped in a vacancy of the Fe-sublattice the nearest atomic environment mainly consists of Al atoms and is different from the environment of a vacancy in the Al sublattice. Therefore, the coincident Doppler broadening technique permits to specify the sublattice on which vacancies are located. Müller et al. conclude from their Doppler-broadened spectra that vacancies are formed on the Fe sublattice. For details, we refer the reader to the review of Sprengel et al. [29]. In what follows we deal with thermal vacancies in Fe-rich Fe-Al alloys, which mainly occur on the Fe sublattice.

Both techniques, differential dilatometry and positron annihilation, have been applied to study vacant lattice sites in thermal equilibrium in Fe-Al phases. We first summarize the differential dilatometry results of Kerl et al. [30] and then continue with the results of Schaefer and co-workers [31] obtained by positron studies.

The vacancy fractions measured by differential dilatometry in three Fe-Al alloys with different composition are shown in Figs. 9a and 9b. Vacancy site fractions between about 10^{-5} and 3 % could be observed. We note that the total vacancy fractions are high and that they increase slightly with Al content:

$$C_V(Fe_{64}Al_{36}) < C_V(Fe_{57}Al_{43}) < C_V(Fe_{50}Al_{50}) \qquad (16)$$

The thermal vacancy fraction is highest in $Fe_{50}A_{50}$. At about 1400 K the fraction is 3×10^{-2} for this alloy. This value is more than one order of magnitude higher than in pure aluminium near its melting temperature (see Fig. 5). The vacancy fractions appear to be correlated with the areas of the Kubaschewski phase diagram. This is indicated in the Figs.9a and b by vertical lines. In the B2' and B2(l) area of the phase diagram vacancy formation obeys Arrhenius laws with a formation enthalpy of about 1 eV and formation entropies of about 4 to 5 times the Boltzmann constant. For higher temperatures, in the B2(h) area, the increase of the vacancy fraction with temperature is slower and can be described by effective formation enthalpies between 0.3 and 0.5 eV. In the disordered A2 phase the vacancy fraction shows again a steeper increase with temperature and an effective formation enthalpy of 1.5 eV has been deduced in [30].

The high thermal vacancy fractions suggest that agglomerates of vacancies such as divacancies or triple defects (two vacancies on the Fe sublattice and one Fe antisite atom on the Al sublattice) contribute to the total defect population. This conclusion is also supported by high defect formation volumes of about 1.4 atomic volumes deduced for $Fe_{60}Al_{40}$ from positron annihilation taken under hydrostatic pressure and reported by Wolff et al. [31]. These authors took this as evidence that thermal defects in the B2-phase are mainly triple defects.

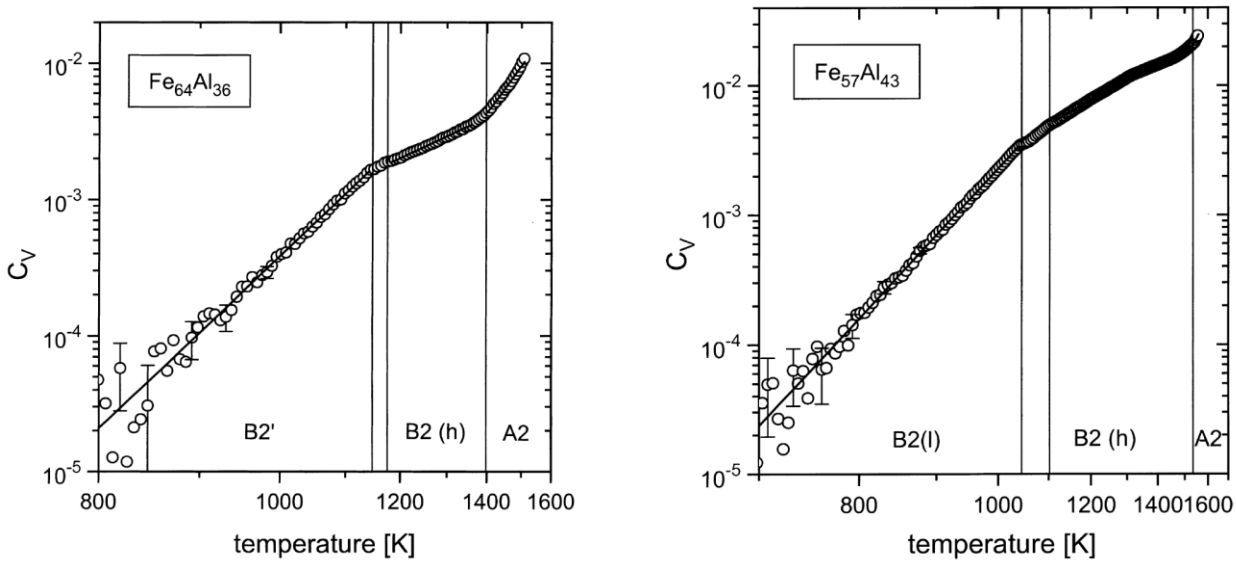

Fig. 9a, b: Vacancy site fractions in thermal equilibrium for $Fe_{64}Al_{36}$ (a: left) and $Fe_{57}Al_{43}$ (b: right) in logarithmic scale obtained from differential dilatometry by Kerl et al. [30]

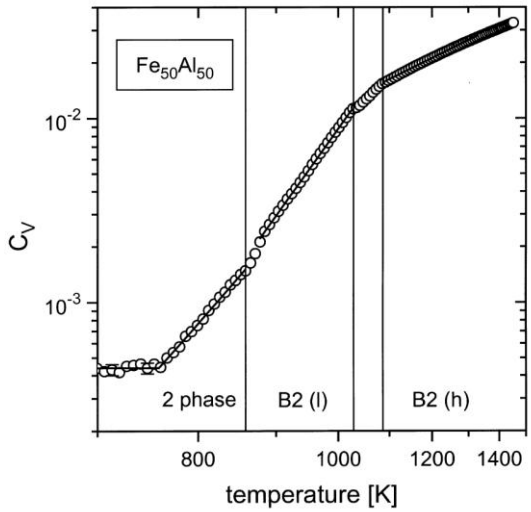

Fig. 9c: Vacancy fraction in thermal equilibrium for $Fe_{50}Al_{30}$ in logarithmic scale obtained from differential dilatometry by Kerl et al. [30]

Positron lifetimes have been reported for Fe_3Al by Schaefer et al. [32] and are displayed in Fig. 10. These measurements pertain to an Fe-Al alloy with higher Fe-content than those alloys studied by differential dilatometry. Figure 10 shows an almost ideal sigmoidal behaviour of the mean positron lifetime, which is typical for positron trapping and annihilation at thermal vacancies. Influences of the structural phase transitions $D0_3$/A2/B2 are hardly visible in these measurements. An influence of B2(l)/B2(h) could not be expected for the alloy studied, because B2(h) exists only at higher Al contents.

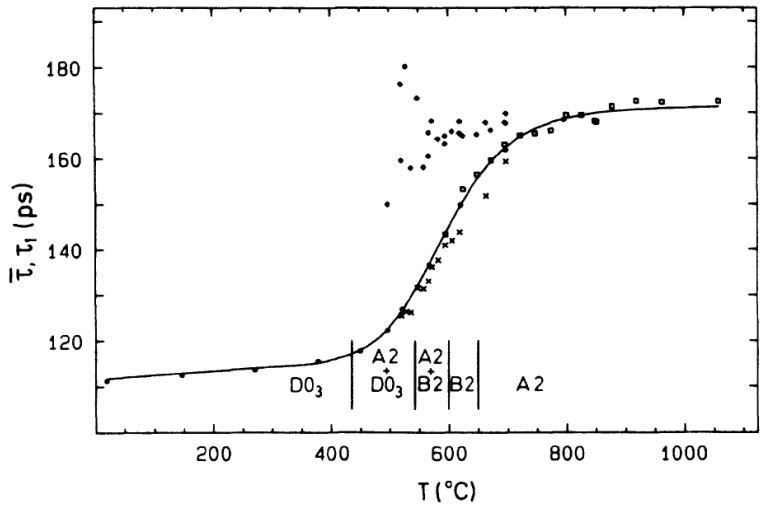

Fig. 10: Positron lifetime in Fe_3Al according to Schaefer et al. [32].

Positron trapping already starts at about 425 °C and saturates at about 900 °C. This start temperature is, relative to the solidus-liquidus temperature of the alloy, much lower than in the case of pure iron (see Fig.4) and suggests for Fe_3Al a rather high level of vacancies in thermal equilibrium. This is in line with the differential dilatometry studies mentioned above. However, the latter cover a wider temperature range and were performed on Al-richer alloys. From a fit of the two-state trapping model to the data of Fig.10 the authors [32] deduce an apparent enthalpy of vacancy formation of about 1.18 eV. With an estimate for the formation entropy of 5 k_B, the authors suggest a vacancy fraction at 1500 °C of about 6.6×10^{-2}. This value is slightly higher than dilatometry values. However, we remind the reader that only the product $\sigma\ exp(S^F/k_B)$, but not the entropy of formation, is directly accessible in positron studies.

Migration of thermal vacancies in Fe-rich iron-aluminides. The complexity of the diffusion processes in ordered iron-aluminides requires knowledge of both thermal vacancy formation as well as vacancy migration. Therefore, also the investigation of vacancy migration in these alloys is of particular interest. Vacancy migration can be assessed by studying equilibration processes. In contrast to pure metals, for iron aluminides the ratio of vacancy migration enthalpy to formation enthalpy is larger than 1 ($H_V^M / H_V^F > 1$) [29], i.e., thermal vacancies form easily, however, are difficult to remove. This fact allows wide time-scales from minutes to hours to days for thermal equilibration studies allowing for measurement techniques such as positron annihilation and dilatometry. In the following dilatometric measurements on B2-$Fe_{61}Al_{39}$ are presented and a comparison is given with data that have been reported earlier on the same alloy composition obtained by positron annihilation [33] and by dilatometric measurements on $Fe_{55}Al_{45}$, an alloy with different composition [34].

Isothermal dilatometry after fast temperature changes seems to be an ideal measurement technique to study point defect kinetics in systems with time constants greater than 10^2s. However, most commercial dilatometers are not designed for long-time, isothermal measurements. For the experimental study presented by the authors an improved, high-precision laser dilatometer has been used that is based on an experimental set-up first applied by Schaefer et al. in [34]. It employs a two-beam Michelson laser interferometer that detects absolute length changes with an accuracy of up to 10 nm of two parallel planes 20 mm apart on the specimen. The present data were obtained using a newly developed force-free sample holder. All measurements were carried out in a vacuum chamber with $p < 10^{-6}$ mbar. For the

temperature measurement three thermocouples were spot-welded along the sample. Temperature control was better than $\Delta T < 0.1$ K. Furthermore, the experimental data are compensated for changes in the environment temperature.

The resulting length-change data in the sample after fast temperature changes can be described by considering two effects: the quasi instantaneous length change caused by the linear thermal expansion and the delayed length change caused by the vacancy migration during the equilibration process. If there is only one vacancy equilibration process, the time dependence of the specimen length after a fast temperature change from an initial temperature, T_i, to a final temperature, T_f, can be described by an exponential function of the form:

$$l = l_0 + l_v(T_i, T_f)[1 - \exp(-t/\tau_E(T_f)] \qquad (17)$$

and from which the equilibration time constant τ_E can be determined. The reciprocal time constants follow an Arrhenius relation of the form:

$$\tau_E^{-1} = \tau_0^{-1} \exp\left(-H_V^M/(k_B T)\right) \qquad (18)$$

from which the migration enthalpy H_V^M and a pre-exponential factor τ_0^{-1} can be obtained.

Figure 1, left panel, shows length-change curves of vacancy equilibration for B2-$Fe_{61}Al_{39}$. The curves are normalized to their l_v values. The initial temperature for every measurement was 973 K and the final equilibration temperatures were 773, 723 and 693 K as indicated in the plot. The form of the equilibration curves suggests a complex equilibration behavior that has to be described by more than one single process. In the present case, a linear combination of Eq. 17 assuming two independent exponential equilibration processes was found most suitable to fit the data. According to this assumption two migration enthalpies can be derived from the measurements. In Fig. 2, right panel, the temperature dependence of the reciprocal time constants is shown as a function of the reciprocal temperature (Arrhenius behavior). The values derived for the enthalpy and the pre-exponential factor of each of the two processes are given in Table 1 together with results of former dilatometric measurement on $Fe_{55}Al_{45}$ [34] and of a positron annihilation study with an alloy of the same concentration as the present one, however, obtained for longer times in a lower temperature regime [33]. In comparison to the value obtained by Schaefer et al. [34] the migration enthalpy obtained from the present study the value for the process with higher activation enthalpy is lower. However, one should take into account that the composition in [34] is slightly different. In [33] only one relaxation mechanism was assumed so a direct comparison with the present data is difficult.

Tab. 1: Comparison of migration enthalpies H_V^M and pre-exponential factors τ_0^{-1} for B2-FeAl alloys obtained from equilibration studies in different temperature regimes by the experimental methods of dilatometry (DIL) and positron annihilation (POS). At higher temperature two equilibration processes are observed.

Alloy	Exp.	T [K]	$H_V^{M_1}$ (eV)	$H_V^{M_2}$ (eV)	$\tau_{0,1}^{-1}$ (s^{-1})	$\tau_{0,2}^{-1}$ (s^{-1})
$Fe_{61}Al_{39}$ [a)]	DIL	693 – 773	1.2 ± 0.3	0.7 ± 0.3	2.7×10^4	2.2
$Fe_{55}Al_{45}$ [b)]	DIL	670 – 791	1.5 ± 0.2	0.6 ± 0.1	4.0×10^5	0.8
$Fe_{61}Al_{39}$ [c)]	POS	623 – 673	1.7 ± 0.2	– [*)]	1.9×10^8	– [*)]

[a)] Present work, [b)] [34], [c)] [33], [*)] in [33] only one process was observed.

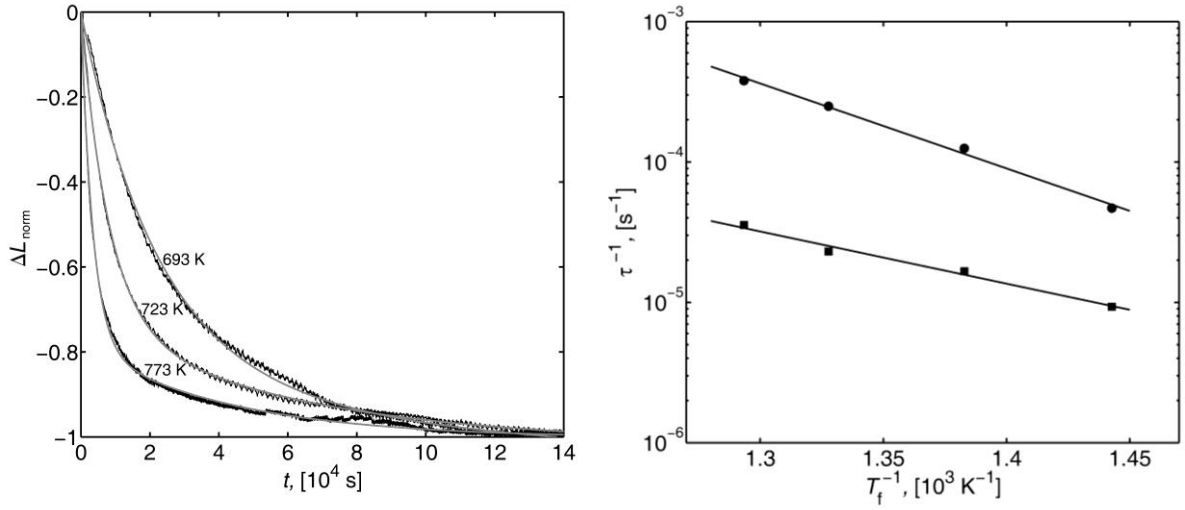

Fig. 11: Left panel: Three normalized length change curves of vacancy equilibration for B2-$Fe_{61}Al_{39}$. The temperatures 693, 723, and 773 K indicate the corresponding equilibration temperatures, T_f, for each curve (see text). The grey lines are fits using a linear combination of two exponentials of the form of Eq. 17. Right Panel: Temperature variation of the inverse time constants $\tau_{0,1}^{-1}$ and $\tau_{0,2}^{-1}$ for equilibration of thermal vacancies. The straight lines are fits according to Eq. 18.

Diffusion in Fe-rich Fe-Al alloys. Tracer diffusion of iron has been studied over wide temperature ranges for three Fe-Al alloys with 25.5, 33, and 48% aluminium by Eggersmann and Mehrer [35] and is displayed in Fig.12. A $Fe_{75}Al_{25}$ alloy was studied by Tökei et al. [36]. The Fe diffusivities in $Fe_{25.5}Al_{74.5}$ from [38] are shown in the upper part of Fig. 12 together with those for $F_{75}Al_{25}$ from [35]. The agreement between the two studies is good.

We note that Fe diffusion, within the B2-ordered area and close to the liquidus temperature, decreases slightly with increasing Al content according to:

$$D(Fe_3Al) > D(Fe_2Al) > D(FeAl) \tag{20}$$

and the pertaining activation enthalpies of Fe diffusion increase with increasing Al content:

$$Q(Fe_3Al) < Q(Fe_2Al) < Q(FeAl). \tag{21}$$

This behaviour is surprising if one considers the Fe-Al phase diagram, which shows that the liquidus temperature decreases with increasing Al content. We also note that the slope of the Arrhenius diagrams changes slightly at the phase transition temperatures and the activation enthalpy of Fe diffusion increases slightly [35]:

$$Q(A2) < Q(B2) < Q(D0_3). \tag{22}$$

The dilatometry data discussed above show a slight increase of the vacant lattice site fractions with increasing Al content. If self-diffusion is promoted by vacant lattice sites, the two results imply that the mobility of diffusion-mediating defects decreases with increasing Al content. In context with the dilatometry results of Figs. 9a to c it is interesting to note that neither the B2'/B2(h) nor the B2(l) /B2(h) transitions, which affect the total vacancy content, is clearly visible in the diffusivities.

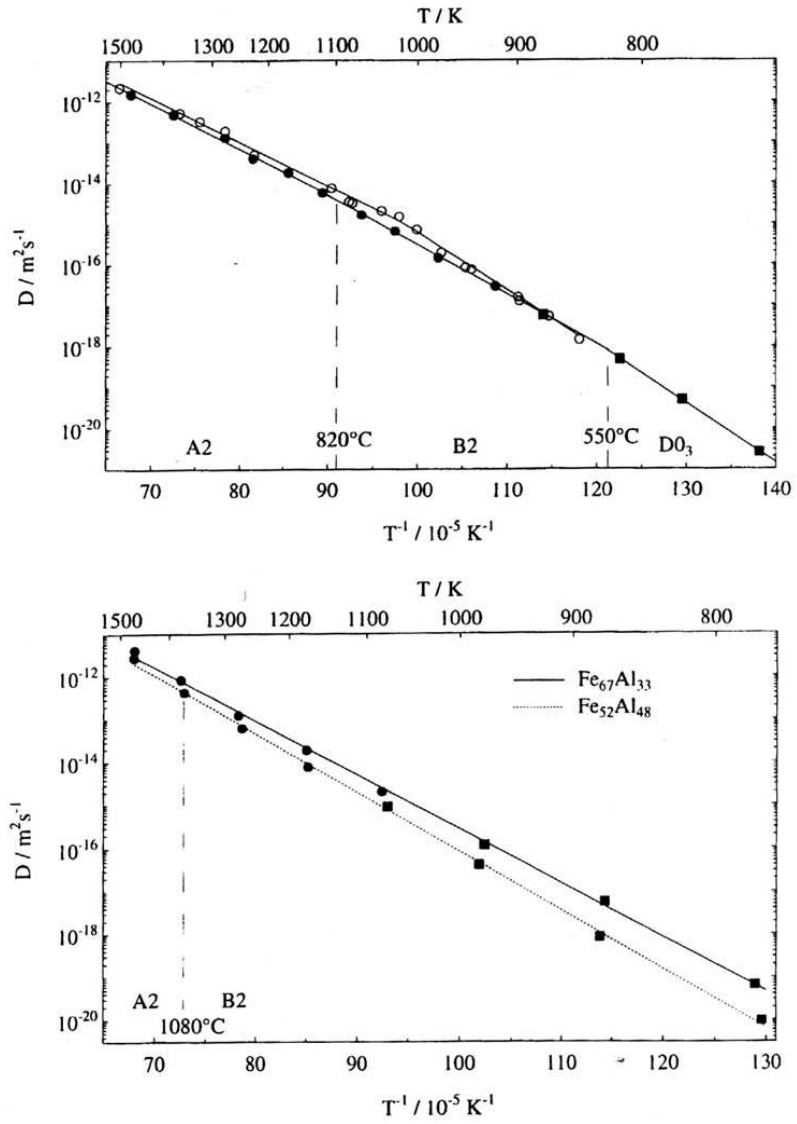

Fig. 12: Upper panel: Tracer diffusion of iron in $Fe_{25.5}Al_{74.5}$ (solid line) from Eggersmann and Mehrer [35]; Iron diffusion in $Fe_{75}Al_{25}$ (open circles) from Tökei et al. [36]. Lower panel: Tracer diffusion of iron in $Fe_{67}Al_{33}$ (solid line) and in $Fe_{52}Al_{48}$ (dotted line) from Eggersmann and Mehrer [35].

There are some additional tracer studies on Fe-Al that should be mentioned for completeness. A fairly early study goes back to Larikov et al. [37]. In this study Fe and Al tracer measurements for several alloy compositions are reported. For Al the tracer ^{26}Al was employed, which was still available at that time. The measurements indicate that Al diffusion is slightly faster than Fe diffusion. However, the data concern a narrow temperature range between about 1200 and 1400 K and are partly inconsistent as discussed in [35]. Therefore, they will not be considered further.

Diffusion coefficients of Fe have also been deduced from Mößbauer spectroscopy data by Vogl and co-workers [38 – 40]. The time/diffusivity 'window' for Mößbauer studies is determined from the lifetime of the ^{57}Fe Mößbauer state, which is 141 ns. The jump rate of the Fe atoms must be in the range of the reciprocal lifetime. This requirement limits Mößbauer data to relatively high temperatures/diffusivities around 1300 K. In the small accessible temperature range the agreement between Mößbauer and tracer data of iron is good [35]. In addition, Mößbauer spectroscopy indicates that Fe atoms jump into an Al site and

back to the Fe sublattice. Close to stoichiometry the time fraction during which Fe atoms occupy Al site is small. With increasing Fe content this time fraction increases. Whether the Fe jumps are caused by isolated vacancies or by agglomerates could not be resolved by the Mößbauer data.

The problem of Al diffusion, which is hindered by the already mentioned lack of a suitable tracer, has been attacked via interdiffusion experiments by Salamon and co-workers [41, 42]. Various interdiffusion couples were prepared and annealed at temperatures between 977 and 1447 K. The diffusion profiles were determined in linear scans parallel to the diffusion direction by electron probe microanalysis. Figure 13 shows two representative examples of interdiffusion profiles. The Matano plane was deduced from the profiles and chosen as origin of the distance coordinate. The profiles were analysed with the Boltzmann-Matano method described above and composition dependent interdiffusion coefficients were obtained. The interdiffusion coefficients show a maximum in the region of the A2-B2 phase transition. Apart from that region they depend only weakly on composition.

The interdiffusion coefficients at the compositions of the three Fe-Al alloys for which Fe tracer diffusivities are available from the work of Eggersmann and Mehrer [35] were used to determine the tracer diffusion coefficients of aluminium from the Darken-Manning equation via (see Eq. 15):

$$D_{Al}^{*} = \frac{D_{\mathrm{int}}}{\Phi S N_{Fe}} - N_{Al} D_{Fe}^{*} \quad . \tag{23}$$

The tracer diffusivities of iron, D_{Fe}^{*}, and the atomic fractions are known from the alloy compositions [35]. In order to apply Eq. 23 the thermodynamic factors is needed as well. Values of the thermodynamic factors are available from semi-empirical calculations by Liubich et al. [43, 44]. The reliability of the theoretical estimates was judged by an investigation of the Kirkendall shift in the diffusion couples by Salamon et al. [41, 42]. Measurements of the Kirkendall shift permit an independent determination of the Al-diffusivity at the composition of the Kirkendall plane. The vacancy wind factor S was estimated and taken into account although it turned out to be a small correction. For details see [41].

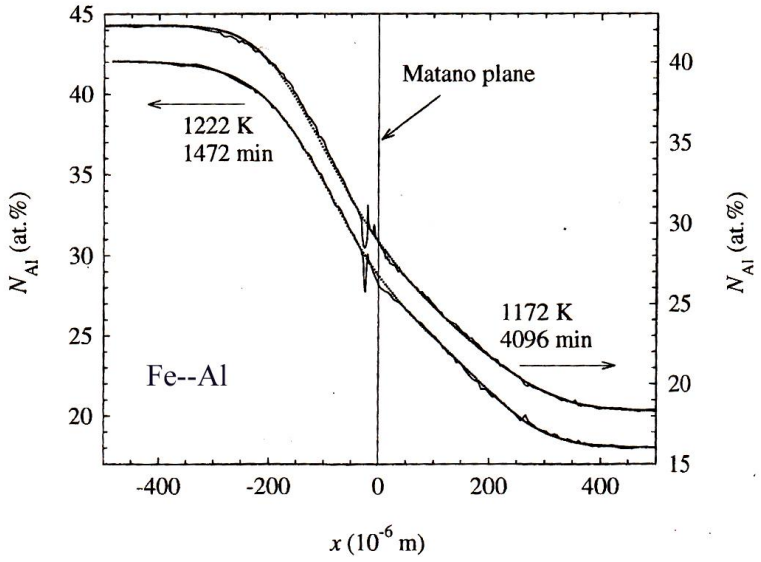

Fig. 13: Interdiffusion profiles of two diffusion couples $Fe_{82}Al_{18}$ – $Fe_{58.3}Al_{41.7}$ measured by electron microprobe scans according to Salamon and Mehrer [41, 42]. The Matano plane is taken as origin of the x-coordinate.

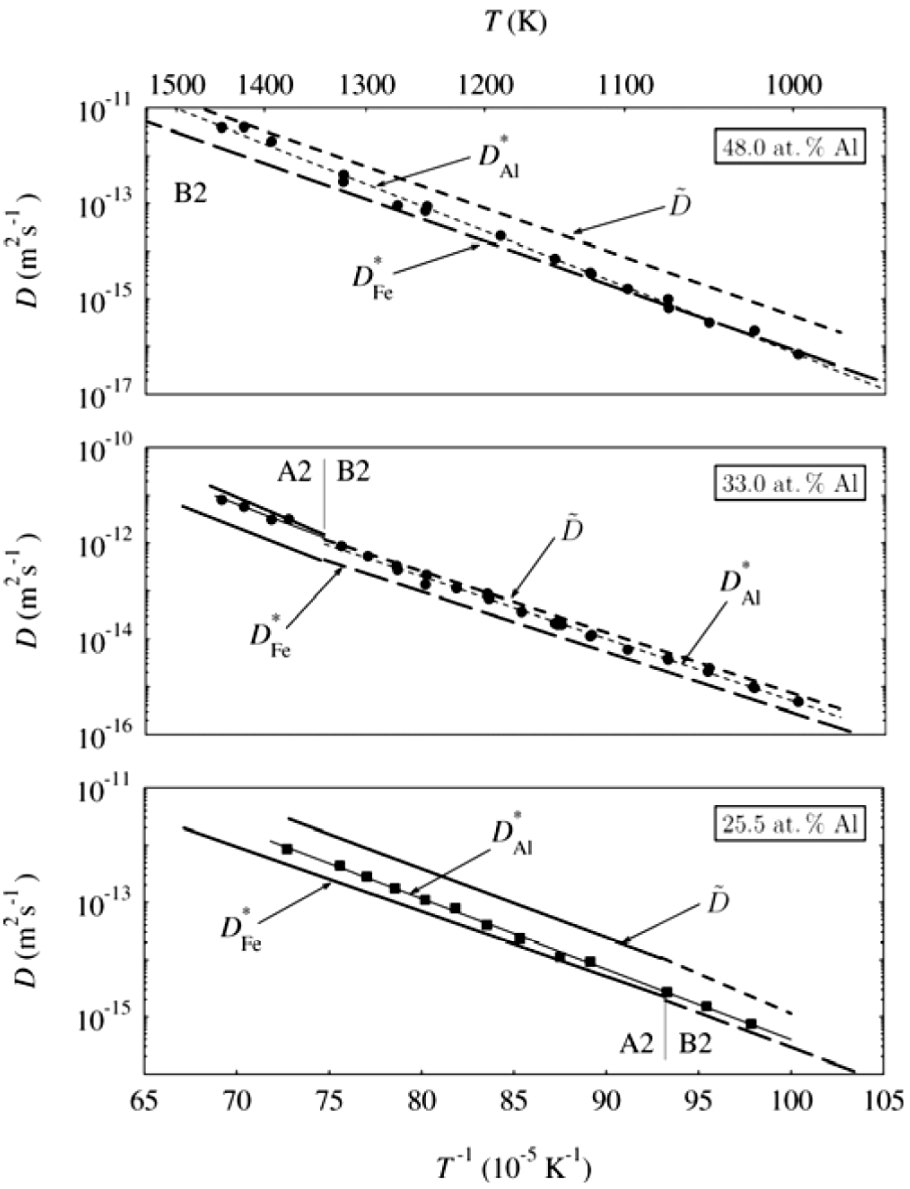

Fig. 14: Arrhenius diagrams of Fe tracer diffusion, interdiffusion coefficients for the three alloys with 25.5, 33 and 48 at. % Al according to Salamon and Mehrer [41]. Symbols indicate Al tracer diffusivities calculated from the Darken-Manning equation (see text).

The Al tracer diffusivities are shown in Fig. 14 together with the interdiffusion coefficients and the Fe tracer diffusivities. We note that for all three alloy compositions investigated, self-diffusion of Fe is slower by less than a factor of two to three than Al self-diffusion. The difference decreases with decreasing temperature and below about 1100 K the self-diffusion coefficient of Fe and Al in the B2 phase are practically the same. This strongly suggests that diffusion of both types of atoms occurs via a mechanism which involves interchanges between the Fe and Al sublattices of the B2 structure.

In a perfectly ordered B2-structure the ratio between the self-diffusivities of the components should lie within narrow limits for the so-called six-jump cycle mechanism illustrated in Fig. 15. For example, for the six-jump cycle in an (110) plane the ratio must lie between 2 and 0.5. However, there are other types of cycles illustrated also in Fig. 15. In addition, Murch and Belova [45] have shown that the strict boundaries may considerably widen if the compositions deviate from stoichiometry, which is the case for the alloys considered above.

The role of agglomerates as diffusion vehicles can also not be excluded. Two vacancies on the Fe sublattice and an Al antisite atom can associate to form a bound triple defect. A triple-defect mechanism based on bound triple defects has been proposed by Stolwijk et al. [46] to operate in the B2 compound CoGa. The triple-defect mechanism is illustrated in Fig. 16. This mechanism also leads to a coupling between the two diffusivities. The limit for the ratio of the two diffusivities is 13.2, which is wider than for the six-jump cycle mechanism in the completely ordered compound.

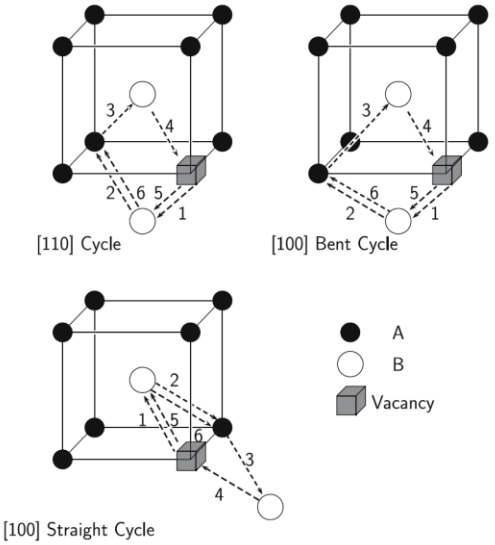

Fig. 15: Six-jump cycle mechanism in a strictly order B2 compound. Three different types of six-jump cycles are indicated**.**

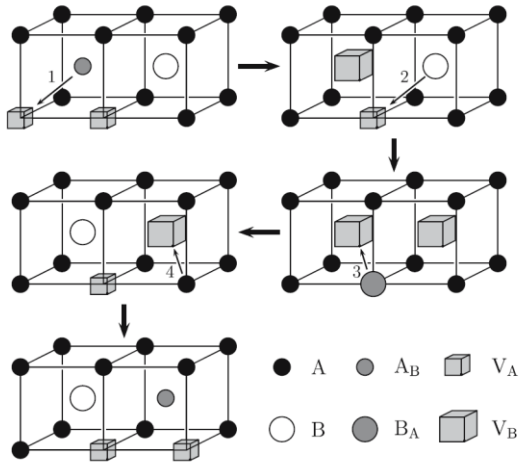

Fig. 16: Triple defect mechanism in a B2-compound.

Solute diffusion in Fe-Al alloys

Solute diffusion in Fe-Al has been investigated by Peteline et al. [47]. It is of interest for ternary alloying elements. In addition, solutes that substitute on the Al sublattice are to some extend suitable to mimic Al self- diffusion. Diffusion of various solutes in Fe_3Al is shown in Fig. 17. Here, Zn and In substitute on the Al sublattice and like Al diffuse slightly faster than Fe and with similar rates as Al. The solutes Co and Ni substitute on the Fe sublattice. They are slower diffusers and have higher activation enthalpies. It is also evident that the structural phase transition B2/A2 has a weak influence on the diffusivity.

The activation enthalpies of the solutes In, Zn, Mn, Co, Ni and that of Fe self-diffusion in this alloy are displayed in Fig.17 (right part) versus the atomic radius of these atoms. A clear correlation of the activation enthalpies with the atomic radius is not obvious. On the other hand, the figure shows that solutes incorporated in Al sublattice (Zn, Mn, Cr, In) have lower activation enthalpies, whereas solutes incorporated in Fe sublattice (Ni, Co) have higher activation enthalpies

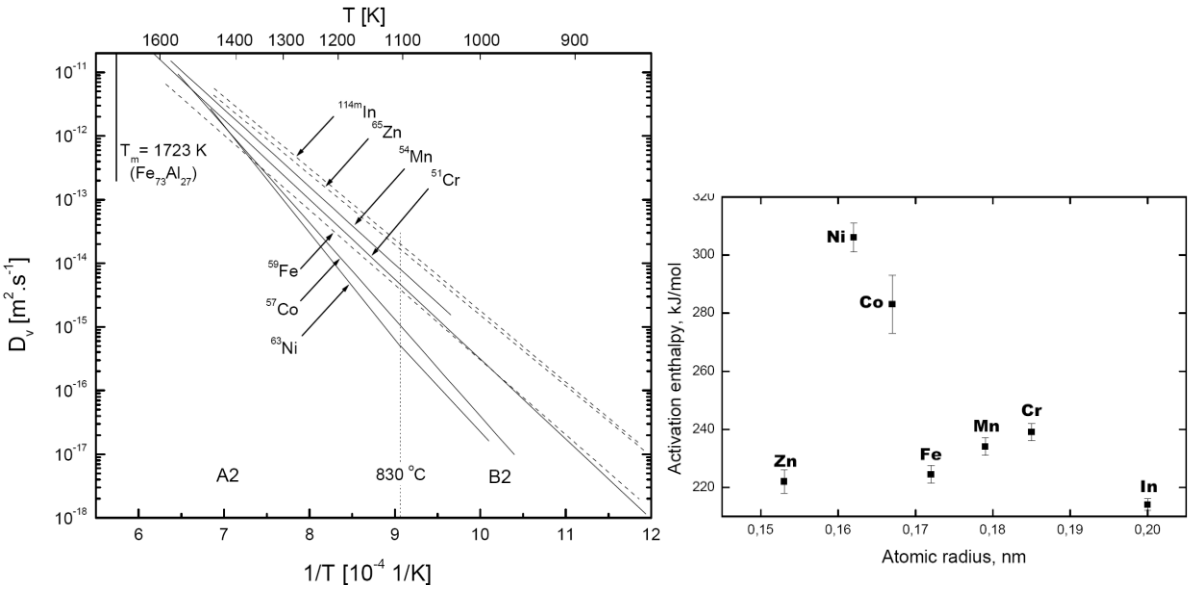

Fig. 17: Left**:** Diffusion of the solutes In, Zn, Mn Cr, Co, Ni and self-diffusion of Fe in Fe_3Al according to Peteline et al. [47]. Right: Activation enthalpies of diffusion of the solutes In, Zn, Mn Cr, Co, Ni and self-diffusion of Fe in Fe_3Al versus the atomic radius.

Acknowledgements

One of the authors (H.M) is grateful to Profs. Sprengel and Würschum for the invitation to join the Institute of Materials Physics at Graz University of Technology, Graz, Austria, as visiting professor in May 2012.

Literature

[1] G. Sauthoff, *Intermetallics*, VCH Verlagsgesellschaft, Weinheim, Germany, 1995.
[2] J. Philibert, *Atom Movements – Diffusion and Mass Transport and Solids*, Les Editions de Physique, Les Ulis, Cedex A, France, 1991.
[3] H. Mehrer, *Diffusion in Solids - Fundamentals, Methods, Materials, Diffusion-controlled Processes*, Springer-Verlag, 2007; Paperback edition 2010.
[4] A. Seeger, H. Mehrer, *Analysis of Self-diffusion and Equilibrium Measurements*, in: Vacancies and Interstitials in Metals, Eds. A. Seeger, D. Schumacher, J. Diehl, and W. Schilling, North-Holland, Amsterdam,, 1970-
[5] A.B. Lidiard, Phil. Mag. **5**, 1171 (1960).
[6] A. D. LeClaire, Philos. Mag. **7**, 141 (1962).
[7] H.-E. Schaefer, Phys. Stat. Sol. (a), 102, 97 (1987).
[8] M. Lübbehusen, H. Mehrer, Acta Metal. Mater. **38**, 283-292 (1990).
[9] Y. Iijima, K. Kimura, K.I. Hirano, Acta Metall. **36**, 2811 (1988).
[10] F. S. Buffington, K.I. Hirano, M. Cohen, Acta Metall. **9**, 434 (1961).
[11] C.M. Walter, N.L. Peterson, Phys. Rev. **178**, 922 (1969).
[12] H.-E. Schaefer, K. Maier, M. Weller, D. Herlach, A. Seeger, J. Diehl, Scripta Metallurgica **11**, 803 – 809 (1977).
[13] K. Maier, H. Metz, D. Herlach, H.-E. Schaefer, J. of Nuclear Materials **69&70**, 589 – 592 (1978).

[14] H. Mehrer (Vol. Ed), *Diffusion in Solid Metals and Alloys*, Landolt-Börnstein, New Series, Vol. 26, Springer Verlag, 1990.
[15] T.S. Lundy, J.F. Murdock, J. Appl. Phys. **33**, 1671 (1962).
[16] R. Messer, S. Dais, D. Wolf, in: Proc. 18th Ampere Congress, P.S. Allen, E.R. Andrew, C.A. Bates (Eds.), Nottingham, England, 1974.
[17] T. F. Volin, R.W. Balluffi, Phys. Status Solidi **25**, 163 (1968).
[18] R.O. Simmons, R.W. Balluffi, Phys. Rev. **129**, 1533 (1963).
[19] G. Bianchi, D. Mallejac, C. Janot, G. Champier, Compt. Rend. Acad. Sci., Paris, **263**, 1404 (1966).
[20] G. Guarini, G.M. Schiavini, Philos. Mag. **14**, 47 (1966).
[21] H.-E. Schaefer, R. Gugelmaier, M. Schmolz, A.Seeger, Materials Science Forum **15-18**, 111-116 (1987).
[22] T. Hoshino, R. Zeller, P.H. Dederichs, Phys. Rev. B **53**, 8971 (1996).
[23] O. Kubaschewski, *Iron-binary phase diagrams*, Berlin, Springer, 1982.
[24] T.B. Massalski, *Binary alloy phase diagrams*, 2nd edition, Materials Park, ASM, 1990.
[25] W. Köster, T. Gödecke, Z. Metallkd. **71**, 765 (1980).
[26] C.L. Fu, Y.Y. Ye,,M.H. Yoo, K.M. Ho, Phys. Rev **B 48**, 6712 (1993).
[27] M. Fähnle, J. Mayer, B. Meyer, Intermetallics **7**, 315 (1999).
[28] M. Müller, W. Sprengel, J. Major, H.-E. Schaefer, Materials Science Forum **363-365**, 85 (2001).
[29] W. Sprengel, M.A. Müller, H.-E. Schaefer, in: *Intermetallics*, Vol.3, Ch-15:*Thermal Defects and Diffusion*, Eds. J.H. Westbrook, R.L. Fleischer, J. Wiley, 2002, p. 275-293.
[30] R. Kerl, J. Wolff, Th. Hehenkamp, Intermetallics **7**, 301-308 (1999).
[31] J. Wolff, M. Franz, A. Broska, Th. Hehenkamp, Defect and Diffusion Forum **143-147**, 239 (1997).
[32] H.-E. Schaefer, R. Würschum, M. Sob, W. Zak, W.Z. Yu, W. Eckert, F. Banhart, Phys. Rev. **B 41**, 11869 (1990).
[33] R. Würschum, C. Grupp, H.-E. Schaefer, Phys. Rev. Lett. **75**, 97 (1995).
[34] H.-E. Schaefer, K. Frenner, R. Würschum, Phys. Rev. Lett. **82**, 948–951 (1999).
[35] M. Eggersmann, H. Mehrer, *Diffusion in Intermetallic Phases of the Fe-Al System*, Philos. Mag. A **80**, 1219 - 1244 (2000).
[36] Zs. Tökei, J. Bernardini, P. Gas, D.L. Beke, Acta Mater. **45**, 541 (1997).
[37] L.N. Larikov, V. Geichenko,V.M Fal'chenko, in; *Diffusion Processes in Ordered Alloys*, New Dehli, Oxonian Press, 1961.
[38] G. Vogl, B. Sepiol, Acta metall. Mater. **42**, 3175 (1994).
[39] R. Feldwisch, B. Sepiol, G. Vogl, Acta metall. Mater.**43**, 2033 (1995).
[40] M. Eggersmann, B. Sepiol, G. Vogl, H. Mehrer, Defect and Diffusion Forum **143-147**, 339 (1997).
[41] M. Salamon, H. Mehrer, *Interdiffusion, Kirkendall Effect and Al Self-Diffusion in Fe-Al Alloys*, Z. Metallkd. **96**, 1 (2005)
[42] M. Salamon, D. Fuks, H. Mehrer, *Interdiffusion and Al Self-diffusion in Iron-Aluminides*, Defect and Diffusion Forum, **237 - 240**, 444 - 449 (2005).
[43] V. Liubich, S. Dorfman, D. Fuks, H. Mehrer, Mat. Trans., JIM, **40**, 132 (1999).
[44] V. Liubich, S. Dorfman, D. Fuks, H. Mehrer, Mat. Sci. Eng. **A 258**, 65 (1998).
[45] I.V. Belova, G.E. Murch, Philos. Mag. **A 82**, 269 (2002).
[46] N.A. Stolwijk, M. van Gend, H. Bakker, Philos. Mag. **A 42**, 283 (1980).
[47] S. Peteline, E. M. Tanguep Njiokep, S. Divinski, H. Mehrer**,** *Diffusion of Solute Elements in Fe_3Al*, Defect and Diffusion Forum, **216 – 217,** 175 – 180 (2003).